04

Study of aqueous dispersions of nanoparticles obtained by pulsed discharge in bidistilled water

© S.V. Makarova, D.I. Subbotin, V.N. Snetov, V.E. Popov, E.A. Pavlova, V.A. Kolikov

Institute for Electrophysics and Electric Power, Russian Academy of Sciences,
St. Petersburg, Russia
e-mail: makarovasvetlana98@mail.ru

Received September 18, 2025
Revised October 29, 2025
Accepted November 13, 2025

Aqueous dispersions of nanoparticles were synthesized by pulsed electrical discharge synthesis in flowing bidistilled water using copper, silver, iron, and bimetallic (Cu/Ag, Cu/Fe, Ag/Fe) electrodes. Comprehensive analysis revealed that the electrode material determines the phase composition of the nanoparticles: copper and iron primarily form oxides (CuO, Fe_3O_4) with crystallite sizes of 9−10 nm, while silver predominantly forms a metallic phase (Ag, 20−72 nm). In bimetallic systems, composites containing both metallic and oxide phases of all components are formed. The ionic fraction in the dispersions was found to be no more than 5% for copper and up to 30% for silver, while the specific electrical conductivity of the dispersions (2.8−12.1 μS/cm) was close to that of bidistilled water. The observed differences are shown to be due to the different thermodynamic stability of the oxides, determined by the standard electrode potentials of the metals. The method allows for the targeted synthesis of nanocomposites with a predetermined phase composition without the use of chemical stabilizers.

Keywords: Nanoparticles, pulsed electrical discharge, aqueous dispersions, phase composition, specific electrical conductivity.

DOI: 10.61011/TP.2026.03.63160.268-25

Introduction

Synthesis of metal and metal oxide nanoparticles is one of the most fast growing areas of modern materials science [1,2]. Unique physical and chemical properties of nanomaterials provided by their high specific surface-to-volume ratio and size effects offer wide prospects for nanotechnology, nanoelectronics, optical, cosmetology, consumer industry applications, and also in biomedicine for diagnostics, photo-thermal and photodynamic therapy, and drug delivery [3–10]. In particular, water dispersions of metal nanoparticles have prolonged microbiological stability [11], and due to magnetic properties of iron oxide nanoparticles, they are used for biomedical applications, including targeted drug delivery [12,13].

Metal nanoparticles are currently produced using various techniques, including chemical and physical impacts and combinations thereof, for example, ultrasound, thermal treatment or mechanical grinding where the produced particles don't have predefined sizes [14]. Analysis of modern nanoparticle characterization methods and related problems is a key aspect [15]. Plasma nanoparticle synthesis processes implementing various approaches are promising techniques. Thus, nanoparticles can be produced from water-salt solutions via spark discharge coming into contact with the electrode surface [16], silver reduction from silver nitrate solution under the action of bipolar pulse discharge [17] or synthesized in chloroauric acid solution under the action of pulsed discharge [18].

Pulse discharge synthesis in bidistilled water flow developed by the Institute for Electrophysics and Electric Power, Russian Academy of Sciences, is one of the promising nanoparticle water dispersion processes [19,20]. Electric arc process for producing water dispersions of metal particles is a promising synthesis technique due to continuous operation and providing nanoparticles with particular sizes and shapes by varying discharge water dispersion, bidistilled water flow rate and temperature [19]. Current research efforts in this area are focused on the search for new synthesis approaches, including the use of surfactants [21]. The benefit of the technique is in its „green" approach that uses bidistilled water as a reaction medium to produce pure dispersions without organic stabilizer impurities. Patterns of nanoparticle formation from various metals and alloys in pulsed plasma conditions are currently being widely investigated [19,22–24]. However, systematic studies that comprehensively correlate the electrode composition (including bimetallic pairs) with phase composition, crystallite sizes, proportion of ion fraction in solution and conductivity of obtained dispersions are still fragmentary.

Compared with such methods as laser ablation and electric conductor explosion, pulsed discharge synthesis in running water has a set of practical benefits: simpler and scalable equipment, continuous process and ability to use unprepared metal electrodes with arbitrary configuration. Key difference is also in formation of complex bimetallic composites directly in a single process without the need for stage synthesis.

The novelty of the work is in comprehensive comparative study that first systematically linked the use of not only monometallic (Cu, Ag, Fe), but also bimetallic pairs of electrodes (Cu/Ag, Cu/Fe, Ag/Fe) in pulsed discharge conditions to phase composition, crystallite sizes, content of ionic species and conductivity of synthesized water dispersions. Such systematic approach provides targeted formation of composition and properties of nanocomposites on the basis of metals and oxides thereof.

The purpose of this study is to investigate comprehensively the effect of electrode material (Cu, Ag, Fe and bimetallic combinations thereof) on the phase and elemental composition, crystallite sizes, content of ionic species in solution and specific conductivity of water dispersions obtained via discharge synthesis in bidistilled water.

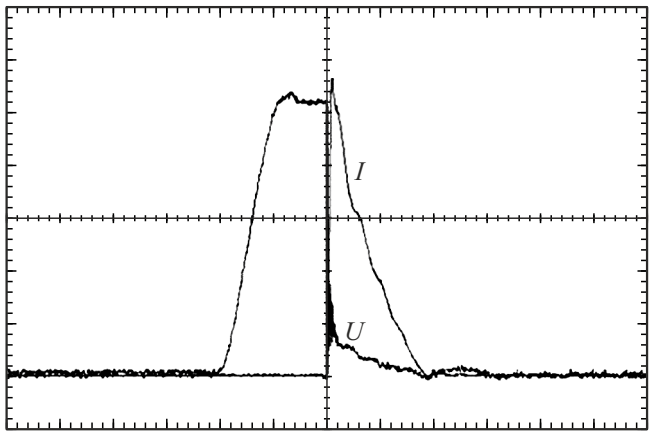

Figure 2. Current pulse waveforms I — 40 A/div, voltage drop across the arc U — 8 kV/div, pulse duration — 5 μs/div.

1. Experimental part

Pulsed discharge synthesis of nanoparticles is based on electrode erosion under the action of spark discharge. Electrode erosion is induced by sudden material heating under the action of electric arc, whose temperature reaches 10 000–20 000 K [22]. Metal transforms into liquid and vapor phases and then is discharged into environment. Flow chart of the setup is shown in Figure 1. Nanoparticle synthesis is performed in the discharge chamber. A pulse with $\sim$ 40 kV, repetition frequency of 100 Hz and amplitude current of $\sim$ 200 A is applied to rod electrodes (high-purity metal wire made of various metals: Cu, Ag, Fe) and induces spark discharge. Bidistilled water is fed to the electric discharge chamber at a flow rate of 26 ml/min perpendicular to the electrode axis. Initial water conductivity is approximately 2.8 μS/cm to provide spark breakdown due to high resistance. For electrodes, 0.7 mm wire consisting of PMM grade electrical copper (at least 99.5 mass %), silver Cp99.99 (at least 99.99 mass %) and steel St20 (at least 98 mass % of iron) was used.

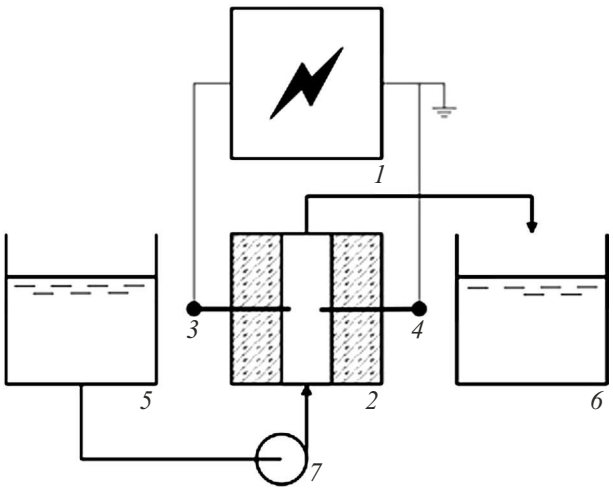

Figure 1. Flow chart of water discharge treatment system: *1* — electric pulse generator; *2* — discharge chamber; *3*, *4* — electrodes; *5* — bidistilled water container; *6* — water dispersion receiving container; *7* — peristaltic pump.

To allow complete description of synthesis energy variables, pulses applied to the electrodes were additionally characterized (Figure 2). Pulse duration was 10 μs, and its waveform was exponentially declining. Total energy enclosed into a single pulse was 2 J, which, at a repetition frequency of 100 Hz, corresponds to a mean power of 200 W and specific energy deposition of $\sim$ 400 J/cm^3. This mode (combination of high voltage, current amplitude and pulse duration) was driven by the need to provide stable breakdown of the interelectrode gap in low-conductivity water, intense electrode erosion to achieve the required nanoparticle output and create a plasma channel with a temperature sufficient for electrode material evaporation.

Nanoparticles are formed during condensation of metal vapor entering the discharge region due to electrode erosion under the action of high temperature on their surface [13].

To form nanostructures as samples, conducting materials (metal wire) were used. Since this work uses bidistilled water, synthesis provides uncontaminated metal and oxide nanoparticles.

Concentration of metals in the prepared dispersions was measured gravimetrically by electrode mass variation. To take into account possible loss of material, the discharge chamber was weighed in dry state before and after the experiment. It has been established that the loss on the chamber walls was max. 5 % of the total electrode mass, and this correction was considered in calculations. Solution conductivity was measured using the ST3 100C conductometer at room temperature with the STCON3 measuring electrode. Measurement range is 2 μS/cm–200 μS/cm. Operating measurement temperature is from 0 °C to 100 °C.

Conductivity measurement accuracy is $\pm$0.5 % of the measured value and $\pm$0.3 °C for temperature. Three-point calibration was used.

Potentiometric measurements were performed using the MULTITEST IPL-101 pH-meter/ion meter, and the

ELIS-131 Cu, ELIS-131 Ag and ESK-1060 combined glass electrodes were used as ion-selective electrodes. Electrodes were prepared and calibrated using calibration solutions. $Cu(NO_3)_2 \cdot 3H_2O$ with a concentration from $10 \cdot 10^{-6}$ to 0.1 M was used as calibration solutions for copper concentration measurement. Similarly, silver concentration was measured using $AgNO_3$ calibration solutions with a concentration from 10^{-6} to 0.1 M. EMF measurement range was from -3000 to 3000 mV. EMF measurement error was within ± 1.0 mV. Temperature error was $\pm 0.5\,^{\circ}$C.

Morphology and elemental composition of the produced nanoparticles were examined using the TESCAN VEGA 3 SBH scanning electron microscope. For the analysis, a concentrated dispersion drop was applied to a silicon substrate and dried in air at room temperature. Measurement was performed using a back-scattered electron (BSE) detector at an accelerating voltage of 20 kV to visualize the contrast by atomic number and identify phases with various elemental compositions.

Crystal structure and phase composition of samples was determined by X-ray diffraction analysis (XRD) using the Rigaku SmartLab 3 diffractometer in CuKα-radiation ($\lambda = 1.5406$ Å). Diffraction patterns were recorded in the range of angles $2\theta = 10-100^{\circ}$ in the Bragg–Brentano configuration using a nickel filter. Test samples were prepared by applying and drying a concentrated dispersion drop to an optical quartz glass slide. Crystallite sizes were calculated by FWHM of reflections using the Scherrer equation.

2. Findings and discussion

The following conducting materials were used for nanostructure analysis: copper, silver, iron and combinations thereof. An iron-iron electrode system has been studied earlier [13] and is not discussed in this work. Each experiment was performed at least three times to ensure repeatability.

The origin of metal ions detected in the solution after the synthesis is an important data interpretation aspect. Not only erosion and condensation processes with nanoparticle formation, but also electrochemical dissolution of metal with transition of cations (Cu^{2+}, Ag^{+}) into the solution take place in the metal electrode–distilled water system in electric discharge conditions. To retain electroneutrality, soluble counterions shall correspond to these cations in the solution. In the plasma-chemical system conditions, nitrate anion (NO_3^-) synthesized from atmospheric nitrogen and oxygen in the plasma channel serves as the main counterion. Hydroxide ions (OH^-) formed in plasma react with metal ions to form insoluble hydroxides that are later transformed into oxides constituting the basis of solid nanoparticles detected by the XRD method.

The origin of metal structures was determined during examination of water dispersions containing material nanoparticles. Conductometry technique was used to measure the electrical conductivity of water dispersions of nanoparticles. Conductometric analysis of the solution has established that samples in liquid state contained the ionic part of the solution having an impact on the electric conductivity. This value grows with time due to absorption from laboratory CO2 atmosphere.

Table 1 shows the data for water dispersions of nanoparticles formed using copper electrodes. The data include copper concentrations in solution measured gravimetrically by the electrode weight variation and copper ion concentrations measured potentiometrically. It can be seen from Table 1 that the specific conductivity, when using copper electrodes, is comparable with that for bidistilled water — 2.8 μS/cm. This suggests that after arc discharge treatment of bidistilled water, a small part of the eroded material transforms into the ionic form of the solution, while the major part remains in the metallic or insoluble oxide/hydroxide forms. The interelectrode gap in this case has virtually no effect on the specific conductivity of the formed water dispersions. Low copper ion concentrations prove that the major part of copper transforms into an insoluble form.

For copper electrodes, a change in the dispersion color from light-green to brown precipitate is observed. This is explained by formation of copper oxide (II).

Table 2 shows the data for water dispersions of nanoparticles formed using silver electrodes. It follows from Table 2 that the samples have a minor excess conductivity, which correlates with the presence of some amount of silver in the ionic form. On the other hand, electric conductivity can be also provided by the presence of metallic silver particles.

When using a combination of copper–silver electrodes, the samples are characterized by a dark gray color close to black with metallic silver impregnations.

Potentiometric measurements haven't detected any copper ions, and small amounts of ionic silver have been detected. With time, silver in the amorphous form in the sample precipitates on the container walls. Comparison of data by concentration for copper and silver measured gravimetrically and potentiometrically is shown in Table 3.

It can be seen from the findings that copper is contained in the prepared solutions predominantly in the form of metal nanoparticles, Cu^{2+} ion fraction doesn't exceed several percentage points of the total eroded electrode mass measured gravimetrically.

For samples on the basis of silver electrodes, the potentiometric measurement of electrodes has shown the ionic phase concentration up to 30 % of the total eroded weight of electrodes.

Analysis of nanoparticles contained in samples prepared from copper electrodes via the XRD technique has identified crystal phases: metal — Cu and oxide — CuO (Figure 3).

Crystallite sizes were determined using the Scherrer equation from the XRD data: CuO — 10 nm, Cu — 42 nm. Mass concentration of crystal phases: 16.3 % of metallic copper and 83.7 % of copper oxide. Note that crystallite sizes measured via XRD characterize the size of coherent

Table 1. Water dispersion properties for samples prepared using copper electrodes

Interelectrode gap, mm	C(Cu), mg/l	C (Cu^{2+}), mg/l	Ion fraction, %	Specific electric conductivity, μS/cm
1	74.5±1.5	1.2±0.1	1.61	3.3
	74.6±1.5	0.6±0.1	0.80	3.1
	81.9±1.6	0.8±0.1	0.98	2.8
	70.8±1.4	0.0	0.00	5.3
2	50.0±1.0	1.6±0.2	3.20	3.7
	61.5±1.2	0.0±0.1	0.00	3.2
	63.5±1.3	1.0±0.1	1.57	2.9
	46.9±0.9	1.0±0.1	2.13	4.3
	53.0±1.1	0.8±0.1	1.51	4.1
	45.6±0.9	1.5±0.2	3.29	6.0
	69.6±1.4	0.0	0.00	6.7
	42.5±0.9	0.0	0.00	5.3
4	38.0±0.8	1.5±0.2	3.95	4.6
5	38.1±0.8	1.8±0.2	4.72	5.6

Table 2. Water dispersion properties for samples prepared using silver electrodes

Interelectrode gap, mm	C(Ag), mg/l	C (Ag^{+}), mg/l	Ion fraction, %	Specific electric conductivity, μS/cm
1	71.0±1.4	10.0±1.0	14.1	11.5
3	50.8±1.0	4.0±0.4	7.9	10.5
	29.3±0.6	6.8±0.7	23.2	8.6
	46.3±0.9	9.3±0.9	20.1	9.2
	79.8±1.6	13.1±1.34	16.4	12.1
5	21.2±0.4	5.4±0.5	25.5	10.7
	49.9±1.0	6.7±0.7	13.4	10.7
	31.2±0.6	9.2±0.9	29.5	7.9
	26.6±0.5	6.0±0.6	22.6	4.1

Table 3. Water dispersion properties for samples prepared using a combination of copper and silver electrodes

Anode/cathode	C(Ag), mg/l	C (Cu), mg/l	C (Ag^{+}), mg/l	C (Cu^{2+}), mg/l	Ion fraction, % Ag/Cu	Specific electric conductivity, μS/cm
Cu/Ag	49.1±1.0	85.4±1.7	1.7±0.2	0.0	3.46/0	10.5

scattering regions and can differ from sizes of individual nanoparticles, which can consist of several crystallites.

The energy-dispersive X-ray spectroscopy technique was also used to measure concentrations of elements (Table 4).

One main component was detected in the crystal phase in a sample (Figure 4) made using silver electrodes — metallic silver with crystallite sizes measured using the Scherrer equation from the XRD data, (72 ± 6) nm. The sample

Table 4. Mass and atomic concentrations of elements measured via energy-dispersive X-ray spectroscopy in samples prepared using copper electrodes

Element	Concentration, mass %		Concentration, at. %	
	Mark 1 (whole sample)	Mark 2	Mark 1 (whole sample)	Mark 2
O	2.27	21.49	8.44	52.08
Cu	97.73	78.51	91.56	47.92
Total	100	100	100	100

Table 5. Mass and atomic concentrations of elements measured via energy-dispersive X-ray spectroscopy in samples prepared using silver electrodes

Element	Concentration, mass%	Concentration, at.%
O	10.74	44.78
Ag	89.26	55.22
Total	100	100

Table 6. Mass and atomic concentrations of elements measured via energy-dispersive X-ray spectroscopy in samples prepared using a combination of copper and silver electrodes

Element	Concentration, mass %	Concentration, at.%
O	40.44	75.75
Cu	39.74	18.74
Ag	19.82	5.50
Total	100	100

Table 7. Mass and atomic concentrations of elements measured via energy-dispersive X-ray spectroscopy in samples prepared using a combination of copper and steel electrodes

Element	Mass concentration, %	Atomic concentration, %
O	30.91	63.03
Fe	21.14	12.35
Cu	47.95	24.62
Total	100	100

Table 8. Mass and atomic concentrations of elements measured via energy-dispersive X-ray spectroscopy in samples prepared using a combination of silver and steel electrodes

Element	Concentration, mass %	Concentration, at. %
O	26.93	65.60
Fe	23.77	16.59
Ag	49.31	17.82
Total	100	100

was black, which suggested that it contained silver oxide in the amorphous form.

It should be noted that the observed quantitative divergence in oxygen concentration between the XRD data (which prove that there are oxide phases) and energy-dispersive X-ray spectroscopy data is methodologically anticipated. Being a powerful tool for analysis of metals, the energy-dispersive X-ray spectroscopy is less accurate for measuring the concentrations of light elements such as oxygen, therefore, this concentration is underestimated on a systematic basis in Tables 4–8. The presence of adsorbed water in the dried samples can be an additional factor affecting the energy-dispersive X-ray spectroscopy data.

High concentration of oxygen and silver atoms has been detected for these samples (Table 5). Narrow and clearly pronounced reflections indicate high crystallinity of the samples.

XRD of a sample (Figure 5) made using a combination of silver and copper electrodes provided a diffraction pattern with typical reflections of pure silver, silver oxide and copper oxide. Ratio of crystal phases in the sample was 70 % of copper (II) oxide, 25 % of silver, 5 % of silver (I) oxide. Crystallite sizes according to the XRD data: CuO — 9 nm; Ag — 28 nm; Ag_2O — 7 nm.

Table 6 shows the elemental analysis data for samples prepared using a combination of copper and silver electrodes. Concentration of oxygen in the sample is highly overestimated and doesn't correspond to a mixture of oxides of the above-mentioned elements. It probably indicates that the sample was dried incompletely and there is water in various forms.

The absence of Cu^{2+} in the Cu/Ag system, despite a higher activity of copper, can be caused by galvanic substitution reactions in the plasma-liquid medium to reduce Cu^{2+} on the surface of silver nanoparticles: $Cu^{2+} + 2Ag^0 \rightarrow Cu^0 + 2Ag^+$.

This assumption requires a separate experimental check.

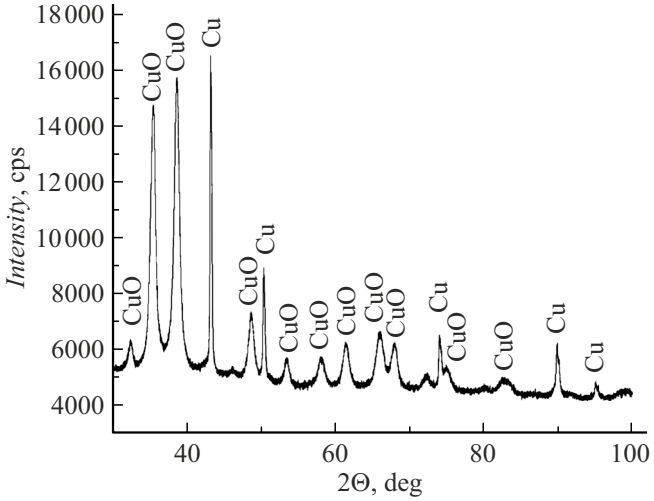

Figure 3. Diffraction pattern of samples prepared using copper electrodes.

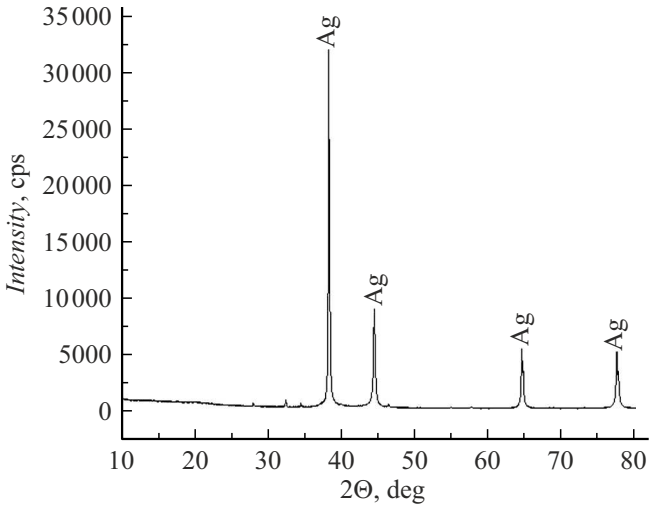

Figure 4. Diffraction pattern of samples prepared using silver electrodes.

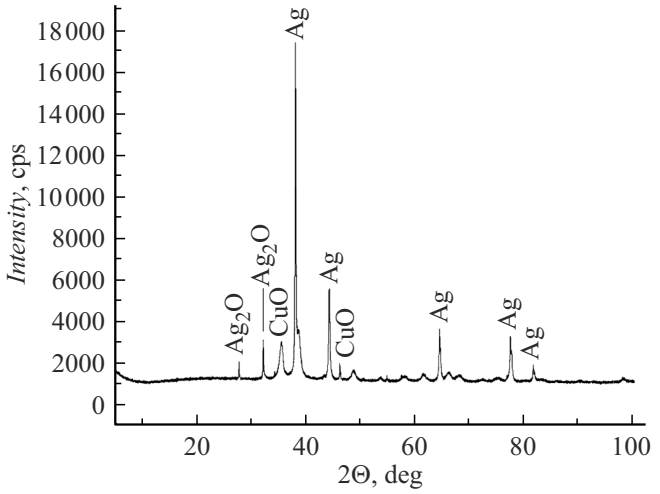

Figure 5. Diffraction pattern of samples prepared using a combination of silver and copper electrodes.

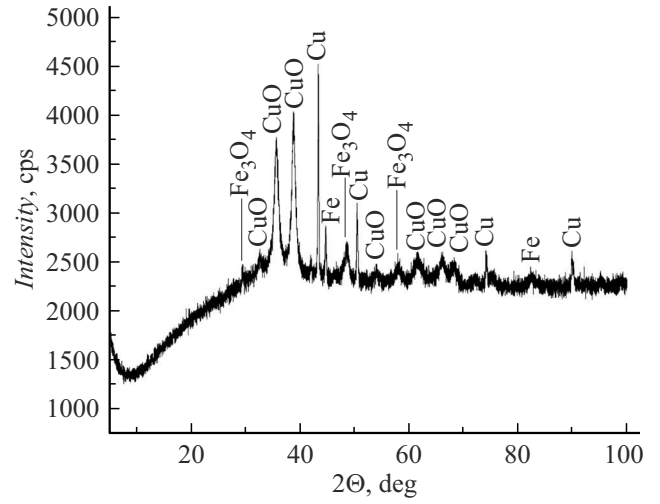

Figure 6. Diffraction pattern of samples prepared using a combination of copper and iron electrodes.

XRD of a sample (Figure 6) prepared using a combination of copper and iron electrodes has detected the concentration of crystal phases — 61% of copper (II) oxide, 25% of iron (IV) oxide, 11% of copper, 2% of iron. Crystallite sizes according to the XRD data: Cu — 55 nm; CuO — 10 nm; Fe_3O_4 (magnetite) — 9 nm.

Table 7 shows the elemental analysis data for samples prepared using a combination of steel and copper electrodes. Similar to the previous sample, concentration of oxygen in the sample is highly overestimated and doesn't correspond to a mixture of oxides of the above-mentioned elements. It probably indicates that the sample was dried incompletely and there is water in various forms.

Reflections of iron and silver oxides, and of pure metals have been also detected in samples prepared using a combination of silver and steel electrodes (Figure 7). The ratio of crystal phases in the sample was: 43% of silver, 31% of iron (III) oxide, 24% of silver (I) oxide, 2% of iron. Crystallite sizes according to the XRD data: Fe — 28 nm; Ag — 20 nm; Ag_2O — 35 nm; Fe_2O_3 (hematite) — 21 nm.

Table 8 shows the elemental analysis data for samples prepared using a combination of steel and silver electrodes.

The observed differences in the phase composition of nanoparticles produced from copper and silver can be explained from the standpoint of thermodynamics and electrochemistry of processes flowing in pulsed plasma conditions.

Copper demonstrates susceptibility to oxide phase (CuO) formation, which agrees with its relatively low standard electrode potential ($E^0(Cu^{2+}/Cu) = +0.34$ V). In conditions of the high-temperature plasma channel and further interaction

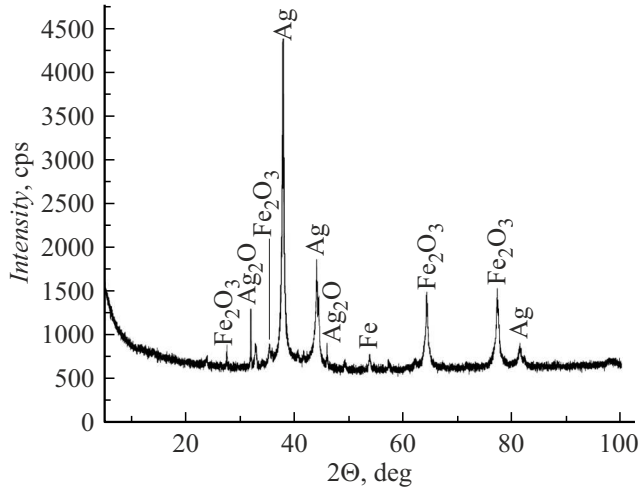

Figure 7. Diffraction pattern of samples prepared using a combination of silver and steel electrodes.

between hot erosion products and water and water vapor, formation of a stable oxide is thermodynamically more beneficial. This is also facilitated by high copper affinity for oxygen.

Unlike copper, silver, having a higher standard potential ($E^0(Ag^+/Ag) = +0.80\,V$), is a nobler metal. Its oxidation is thermodynamically less beneficial. As a result of fast cooling and vapor condensation in water medium, metallic silver is the main phase, which is able to crystallize. While formation of silver oxide (Ag_2O) is probably limited by kinetic factors and occurs to a far lesser extent, and low stability of silver oxide can result in further decomposition.

Thus, the electrode composition predetermines the phase composition of synthesized nanoparticles through their electrochemical properties and thermodynamic stability of potential compounds.

The TESCAN VEGA 3 SBH scanning electron microscope was used to make nanoparticle microphotographs of samples prepared via the electric arc technique with various electrodes (Figure 8): copper (Figure 8, *a*), silver (Figure 8, *b*) and combinations of copper–silver electrodes (Figure 8, *c*), copper–steel electrodes (Figure 8, *d*) and silver–steel electrodes (Figure 8, *e*).

The BSE detector was used for analysis of samples examined on the scanning electron microscope. Microphotographs of samples prepared from copper electrodes (Figure 8, *a*) show that the sample surface contains small impregnations and the sample composition corresponds to two substances (metallic copper and copper II oxide), which have been found by XRD.

A microphotograph in Figure 8, *b* shows a large piece of separated metallic silver and the rest of the sample looks amorphous. This, together with XRD, indicates that metallic silver and probably silver oxide, Ag_2O, have formed.

A sample made from copper and silver electrodes (Figure 8, *c*) contains at least two phases, one of which is metallic silver, and the second one is a mixture of oxides of initial metals. According to XRD, no more complex oxide systems have been found in the crystal phase. Particles with subtle differences in elemental composition are observed in copper–iron system (Figure 8, *d*) and silver–iron system (Figure 8, *e*).

It should be noted that this study has been focused on a complex analysis of phase and elemental composition, and colloidal properties of dispersions. Therefore, quantitative analysis of particle size distribution according to SEM images and direct comparison with coherent scattering region sizes measured using the Scherrer equation haven't been performed. This area is of key interest for future study because it will allow more detailed examination of nanoparticle nucleation and growth process kinetics in pulsed discharge synthesis conditions. DLS measurement of hydrodynamic sizes of nanoparticles and detailed morphological analysis via transmission electron microscopy constitute a separate research task and a subject of our future investigations.

Conclusions

Comprehensive analysis of water dispersions of nanoparticles synthesized via the electric discharge technique using copper, silver, iron and bimetallic electrodes gave the following main findings.

1. The key effect of electrode material on the phase composition of nanoparticles has been established. It is shown that copper and iron predominantly form oxide phases (CuO, Fe_3O_4), while silver mainly forms a metallic phase (Ag). For bimetallic pairs (Cu/Ag, Cu/Fe, Ag/Fe), complex composites are formed that contain both metallic and oxide phases of all components.

2. The origin of differences in the phase composition in terms of thermodynamics and electrochemistry has been explained. It is shown that copper susceptibility to oxidation is caused by a relatively low standard electrode potential ($+0.34\,V$) and high affinity for oxygen in plasma discharge conditions. Nobility of silver ($E^0 = +0.80\,V$) makes formation of silver oxides less thermodynamically beneficial, leading to predominance of a metallic phase.

3. Crystallite sizes were measured for the main phases: CuO (9–10 nm), metallic Cu (42–55 nm), Ag (20–72 nm), Ag_2O (7–35 nm), Fe_3O_4 (9 nm). Oxide crystallite size turned out to be consistently smaller (less than 35 nm) than that of metallic phases, indicating that nucleation and growth mechanisms in the plasma process are different.

4. Potentiometry was used to determine low concentration of ionic species in water dispersions. Ion fraction in the total mass of eroded material is not higher than 5 % for copper and reaches 30 % for silver, which correlates with their different susceptibility to oxidation.

5. It is shown that specific conductivity of the synthesized dispersion is close to that of bidistilled water (2.8–12.1 μS/cm), which additionally proves that nonionic

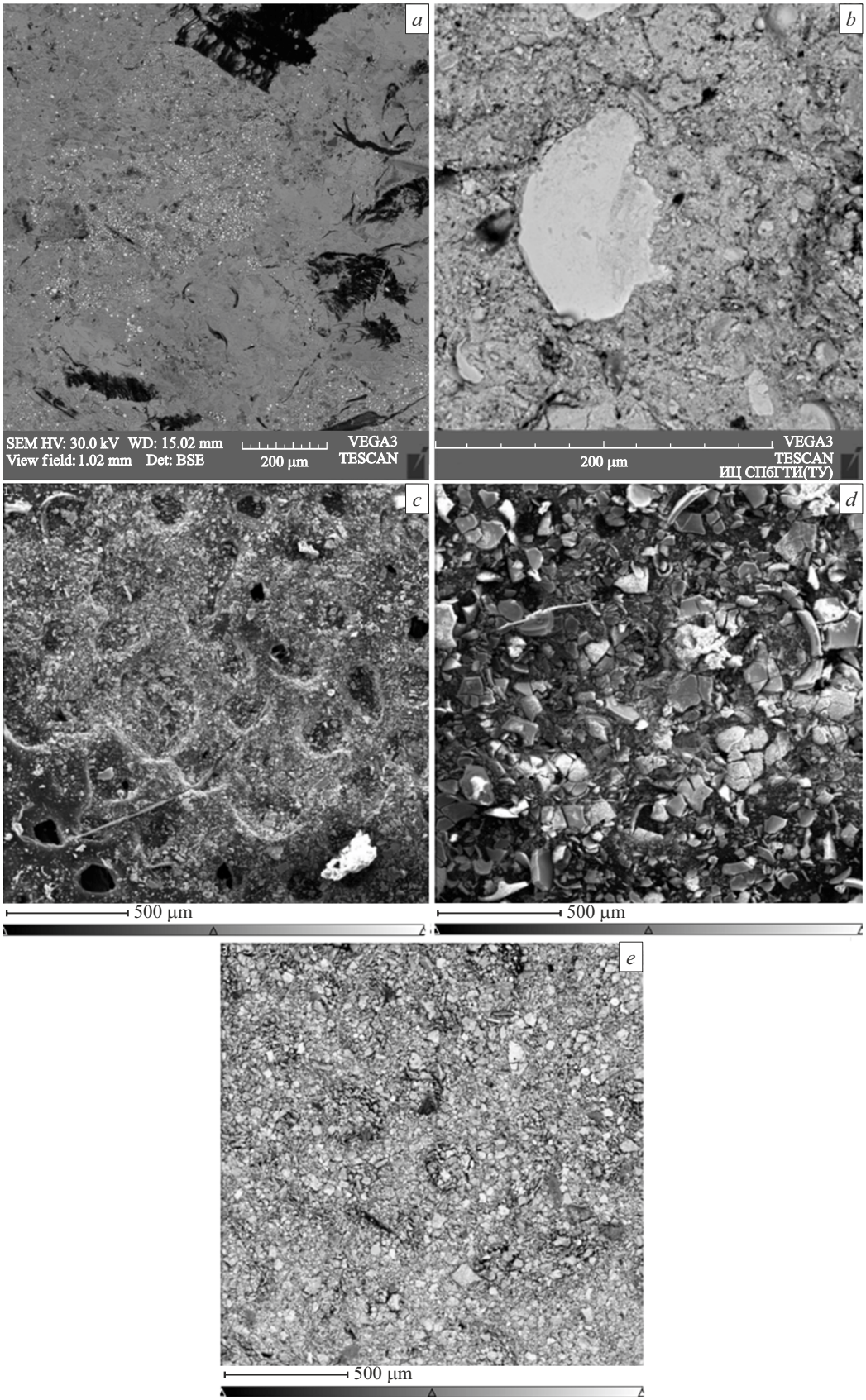

Figure 8. Images recorded using the back-scattered electron detector for copper nanoparticles (*a*), silver nanoparticles (*b*), copper and silver nanoparticles (*c*), copper and iron nanoparticles (*d*), silver and iron nanoparticles (*e*).

(metallic and oxide) forms of nanoparticles prevail in the solution.

Conflict of interest

The authors declare no conflict of interest.

References

[1] S. Mourdikoudis, R.M. Pallares, N.T.K. Thanh. Nanoscale, **10**, 12871 (2018). DOI: 10.1039/C8NR02278J

[2] S. Gavas, S. Quazi, T.M. Karpiński. Nanoscale Res. Lett., **16**, 173 (2021). DOI: 10.1186/s11671-021-03628-6

[3] J. Wang, X. Wu, P. Shen, J. Wang, Y. Shen, Y. Shen, J. Deng. Intern. J. Nanomedicine, **15**, 1903 (2020). DOI: 10.2147/IJN.S239751

[4] S.C. Baetke, T. Lammers, F. Kiessling. British J. Radiology, **88** (1054), 20150207 (2015). DOI: 10.1259/bjr.20150207

[5] B. Klębowski, J. Depciuch, M. Parlińska-Wojtan, J. Baran. Intern. J. Molecular Sci., **19** (12), 4031 (2018). DOI: 10.3390/ijms19124031

[6] E. Radzikowska-Bëchner, W. Flieger, S. Pasieczna-Patkowska, W. Franus, R. Panek, I. Korona-Głowniak, K. Suśniak, B. Rajtar, Ł. Świątek, N. Żuk, A. Bogucka-Kocka, A. Makuch-Kocka, R. Maciejewski, J. Flieger. Molecules, **28** (14), 5519 (2023). DOI: 10.3390/molecules28145519

[7] C. Karuppusamy, P. Venkatesan. J. Pharmaceutical Sci. Res., **9** (3), 318 (2017).

[8] E.S. Shitova, F.V. Makarov, A.A. Pertsev, A.P. Ponomarenko, A.A. Shtraus. Nanoindustry, **16** (1), 30 (2023). DOI: 10.22184/1993-8578.2023.16.1.30.40

[9] C.S.C. Santos, B. Gabriel, M. Blanchy, O. Menes, D. García, M. Blanco, N. Arconada, V. Neto. Mater. Today: Proceed., **2** (1), 456 (2015).

[10] A. Shrestha, A. Kishen. J. Endodontics, **42** (10), 1417 (2016). DOI: 10.1016/j.joen.2016.05.021

[11] V.A. Kolikov, A.F. Rutberg, F.G. Rutberg, V.N. Snetov, A.Yu. Stogov, V.E. Kurochkin, L.K. Panina. Tech. Phys., **52** (2), 263 (2007). DOI: 10.1134/S1063784207020193

[12] F.G. Rutberg, V.A. Kolikov, V.N. Snetov, D.I. Subbotin, V.E. Kurochkin, V.G. Mal'tsev. Tech. Phys., **57** (12), 1661 (2012). DOI: 10.1134/S1063784212120249

[13] F.G. Rutberg, V.A. Kolikov, V.N. Snetov, D.I. Subbotin, A.I. Zhernovoi, I.A. Cherepkova, S.V. Dyachenko. High Temperature, **54** (2), 170 (2016). DOI: 10.1134/S0018151X16020188

[14] M. Shahalaei, A.K. Azad, W.M.A.W. Sulaiman, A. Derakhshani, E.B. Mofakham, M. Mallandrich, V. Kumarasamy, V. Subramaniyan. Frontiers Chem., **12**, 1398979 (2024). DOI: 10.3389/fchem.2024.1398979

[15] V.A. Nadtochenko, M.A. Radtsig, I.A. Khmel'. Nanotechnologies in Russia, **5** (5), 454 (2010). DOI: 10.1134/S199507801005013X

[16] A.M. Orlov, I.O. Yavtushenko, D.S. Bodnarskii. Tech. Phys., **60** (5), 710 (2015). DOI: 10.1134/S1063784215050199

[17] A. Treshchalov, S. Tsarenko, T. Avarmaa, R. Saar, A. Lõhmus, A. Vanetsev, I. Sildos. Plasma Medicine, **6** (1), 85 (2016).

[18] B. Oruncak, M. Özkan, A. Akyüz. Arabian J. Geosciences, **13**, 685 (2020). DOI: 10.1007/s12517-020-05688-x

[19] F.G. Rutberg, V.A. Kolikov, V.N. Snetov, A.Yu. Stogov, V.V. Gusarov, I.P. Voskresenskaya, I.A. Cherepkova. Tech. Phys., **57** (12), 1641 (2012). DOI: 10.1134/S1063784212120237

[20] F.G.Gutberg, V.A.Kolikov, V.E.Kurochkin, V.G.Maltsev. Patent № 2272697 C1 Rossiiskaya Federatsiya, MPK B22F 9/14. *Sposob proizvodstva nanochastits* (№ 2004127426/02 : zayavl. 07.09.2004 : opubl. 27.03.2006)

[21] A.V. Nominé, Th. Gries, C. Noel, A. Nominé, V. Milichko, T. Belmonte. J. Appl. Phys., **130** (15), 151101 (2021). DOI: 10.1063/5.0040587

[22] V.A. Kolikov, M.E. Pinchuk, A.G. Leks, P.G. Rutberg. Proceedings SPIE, **6279**, 62795C (2007). DOI: 10.1117/12.725381

[23] F.G.Rutberg, M.V.Dubina, V.A.Kolikov, A.N.Bratsev, A.V.Shteinberg. DAN, **421** (2), 274 (2008) (in Russian).

[24] A. Dror-Ehre, H. Mamane, T. Belenkova, G. Markovich, A. Adin. J. Colloid Interface Sci., **339** (2), 521 (2009). DOI: 10.1016/j.jcis.2009.07.052

Translated by E.Ilyinskaya